Macromolecules

ARTICLE

pubs.acs.org/Macromolecules

Viscoelastic Properties, Ionic Conductivity, and Materials Design Considerations for Poly(styrene-*b*-ethylene oxide-*b*-styrene)-Based Ion Gel Electrolytes

Sipei Zhang,[†] Keun Hyung Lee,[†] Jingru Sun,[†] C. Daniel Frisbie,*[,†] and Timothy P. Lodge*[,†,§]

[†]Department of Chemical Engineering and Materials Science, University of Minnesota, Minneapolis, Minnesota 55455, United States

[§]Department of Chemistry, University of Minnesota, Minneapolis, Minnesota 55455, United States

Supporting Information

ABSTRACT: The viscoelastic properties and ionic conductivity of ion gels based on the self-assembly of a poly(styrene-*b*-ethylene oxide-*b*-styrene) (SOS) triblock copolymer ($M_{n,S}$ = 3 kDa, $M_{n,O}$ = 35 kDa) in the ionic liquid 1-ethyl-3-methylimidazolium bis(trifluoromethylsulfonyl)amide ([EMI][TFSA]) were investigated over the composition range of 10−50 wt % SOS and the temperature range of 25−160 °C. The poly(styrene) (PS) end-blocks associate into micelles, whereas the poly(ethylene oxide) (PEO) midblocks are well-solvated by this ionic liquid. The ion gel with 10 wt % SOS melts at 54 °C, with the longest relaxation time exhibiting a similar temperature dependence to that of the viscosity of bulk PS. However, the actual values of the gel relaxation time are more than 4 orders of magnitude larger than the relaxation time of bulk PS. This is attributed to the thermodynamic penalty of pulling PS end-blocks through the PEO/[EMI][TFSA] matrix. Ion gels with 20−50 wt % SOS do not melt and show two plateaus in the storage modulus over the temperature and frequency ranges measured. The one at higher frequencies is that of an entangled network of PEO strands with PS cross-links; the modulus displays a quadratic dependence on polymer weight fraction and agrees with the prediction of linear viscoelastic theory assuming half of the PEO chains are elastically effective. The frequency that separates the two plateaus, ω_c, reflects the time scale of PS end-block pull-out. The other plateau at lower frequencies is that of a congested micelle solution with PS cores and PEO coronas, which has a power law dependence on domain spacing similar to diblock melts. The ionic conductivity of the ion gels is compared to PEO homopolymer solutions at similar polymer concentrations; the conductivity is reduced by a factor of 2.1 or less, decreases with increasing PS volume fraction, and follows predictions based on a simple obstruction model. Our collective results allow the formulation of basic design considerations for optimizing the mechanical properties, thermal stability, and ionic conductivity of these gels.

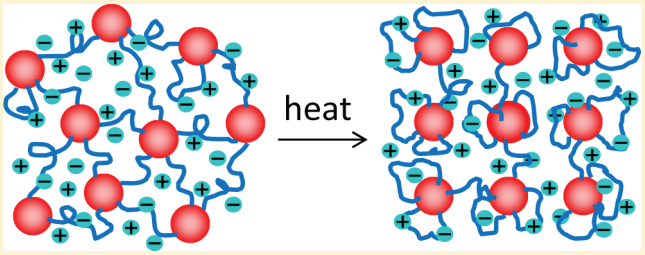

INTRODUCTION

Ionic liquids have attracted considerable interest in recent years due to their unique combination of properties such as negligible vapor pressure, nonflammability, exceptional thermal and electrochemical stability, and optical transparency, as well as high ionic conductivity.[1−4] These properties make ionic liquids viable electrolytes for electrochemical devices including dye-sensitized solar cells,[5−7] electromechanical actuators,[8−10] supercapacitors,[11−15] lithium ion batteries,[16−18] and organic thin film transistors.[19−24] Additionally, the numerous choices of component ions impart flexibility in materials design to fulfill property requirements.

From an applications standpoint, providing ionic liquids with mechanical integrity without too much sacrifice in transport properties (e.g., ionic conductivity) is desirable. Both low molecular weight gelators[25,26] and macromolecules[27,28] have been utilized to achieve this goal. Specifically, solid polymer electrolytes[29] incorporating ionic liquids, alternatively termed ion gels, are advantageous due to their higher ionic conductivity (ca. 10^{-3} S/cm at 25 °C)[30] than conventional lithium salt electrolytes such as PEO/$LiClO_4$ (ca. 10^{-5} S/cm at 25 °C).[31] A commonly employed method to form network structures for ion gels is cross-linking, which can be realized by either chemically reacting (macro)monomers with functional cross-linkers[32−38] or forming physically associated cross-links.[39−43] Physical cross-linking utilizing block copolymers is a particularly versatile route due to the ease in tuning morphologies and properties through variations of block length and sequence. For instance, the self-assembly of an ABA triblock copolymer with an ionic liquid soluble B block and insoluble A blocks can produce a network with A cross-links and a continuous B/ionic liquid phase.

There have been relatively few reports describing both mechanical properties and ionic conductivity of ion gels. In terms of chemically cross-linked systems, Matsumoto and Endo prepared

Received: June 15, 2011
Revised: October 5, 2011
Published: October 28, 2011

epoxy-based ion gel films containing ammonium/imidazolium bis(trifluoromethylsulfonyl)amide ([TFSA]), and measured ionic conductivity as well as tensile properties for different compositions at room temperature.[36,37] For physically cross-linked systems, the temperature dependence of the modulus is more interesting since cross-links are formed by noncovalent interactions such as hydrogen bonds or thermodynamic incompatibility between certain components. We reported the first ion gels based on ABA triblock copolymers.[39] The self-assembly of poly(styrene-*b*-ethylene oxide-*b*-styrene) (SOS) in the ionic liquid 1-butyl-3-methylimidazolium hexafluorophosphate ([BMI][PF_6]) was found to form a soft gel with the addition of as little as 4 wt % SOS, and the ionic conductivity of gels with 5 and 10 wt % SOS was minimally reduced from the neat ionic liquid over the temperature range of 10−90 °C. We further developed thermoreversible ion gels with a different end-block in another ionic liquid, 1-ethyl-3-methylimidazolium ([EMI]) [TFSA], and measured the ionic conductivity and modulus of the gel with 10 wt % polymer.[40] However, these two studies merely focused on modulus in dilute systems and ionic conductivity at one or two compositions. More systematic studies of both mechanical and electrical properties of ion gels are desirable.

This work is a continuation of our effort to understand viscoelastic and ionic motions in ion gels based on SOS and poly(styrene-*b*-methyl methacrylate-*b*-styrene) (SMS) in [EMI][TFSA]. In terms of ionic motions, we have reported the effect of polymer concentration, temperature, and midblock identity on ionic conductivity and double-layer capacitance.[30,44] In terms of viscoelastic motions, the focus of the previous report was on SMS based gels.[44] In this work, we report the viscoelastic properties of gels formed with SOS over wide temperature and concentration ranges. Although the viscoelastic properties of these gels appear qualitatively similar to those based on SMS reported previously,[44] a difference in molecular weight of the end-blocks between SOS and SMS leads to a rather different physical picture. Additionally, here we employ a new method to analyze the effect of polymer concentration on ionic conductivity by comparing the gels with homopolymer solutions, which clearly illustrates the role of the insulating poly(styrene) (PS) cross-links in obstructing ionic motion.

EXPERIMENTAL SECTION

Materials. The SOS, SMS, poly(methyl methacrylate) (PMMA) polymers, and [EMI][TFSA] were synthesized and characterized as previously reported.[44,45] We denote the polymers as SOS(3−35−3), SMS(18−86−18), and PMMA(126), with the numbers in parentheses indicating the number-average molecular weights in kg/mol. The poly(ethylene oxide) (PEO) polymer used to prepare PEO/[EMI][TFSA] solutions was the precursor for the synthesis of SOS(3−35−3), and is thus denoted as PEO(35).

All ion gels and homopolymer solutions were prepared by mixing weighed amounts of the respective polymer and the ionic liquid in CH_2Cl_2 cosolvent. After stirring for 2 h, the mixtures were purged with nitrogen gas for a day to evaporate most of the cosolvent. Finally, the samples were placed in a vacuum oven at ca. 70 °C for 2 days to completely remove the cosolvent. To avoid any effects of moisture, all samples were kept in a vacuum desiccator and were dried in a vacuum oven at ca. 70 °C for a day before any measurements were carried out.

Rheology and Impedance Spectroscopy. Rheological and impedance measurements were conducted on an ARES rheometer (Rheometric Scientific) connected to an Agilent 4284A LCR bridge (TA Instruments), using parallel plate geometry. Depending on the modulus, both 50 and 25 mm diameter plates were employed. For samples in need of 50 mm plates, i.e., gels with 10 wt % polymer, the solution with 5 wt % PMMA(126), and the solution with 8 wt % PEO(35), impedance measurements were conducted on a different piece of equipment. Otherwise, both impedance and rheology measurements were performed on the same sample with a gap spacing of ca. 1 mm. At each temperature, the sample was thermally equilibrated for 15−20 min and the gap was adjusted to compensate for the thermal expansion of the tool set, then the dynamic shear moduli were examined in the linear viscoelastic regime, followed by measurements of complex impedance while maintaining a shear frequency of 10 rad/s using an AC signal of 0.1 V amplitude in the electrical frequency range of $20-2 \times 10^6$ Hz. The shear frequency was set to 10 rad/s because the instrument requires that impedance data be recorded at a finite shear frequency. There was no dependence of impedance on shear frequency between 1 and 100 rad/s. Temperatures were controlled to within 0.2 °C of the set points with an environmental control circulator under a nitrogen atmosphere. Measurements were taken at a series of decreasing temperatures. Ionic conductivity was determined from the high frequency plateau of the real part of complex conductivity, as was reported previously.[44]

For gels with 10 wt % polymer, the solution with 5 wt % PMMA(126), and the solution with 8 wt % PEO(35), impedance measurements were performed with a homemade cell using a Solartron 1255B frequency response analyzer connected to a Solartron SI 1287 electrochemical interface. Frequency sweeps were conducted from 1 to 10^6 Hz with an AC amplitude of 10 mV. The cell is composed of a Teflon spacer with an inner diameter of 4 mm and a thickness of 2 mm sandwiched between two platinum coated stainless steel electrodes. Temperatures were controlled to within 0.5 °C of the set points with a thermostated water bath. The samples were thermally equilibrated for ca. 30 min prior to the measurements. Conductivity of a sample with 10 wt % SMS(18−86−18) was cross-checked; the value obtained from this instrument agrees with that measured on ARES at room temperature.

Small Angle X-ray Scattering. Small-angle X-ray scattering (SAXS) experiments were performed at the DuPont-Northwestern-Dow collaborative access team (DND-CAT) beamline at the Advanced Photon Source, Argonne National Laboratories. Samples were sealed in DSC pans, which were heated in a Linkam DSC sample holder during scattering experiments. For the gel with 40 wt % SOS(3−35−3), measurements were performed with an annealing time of 5 min at each temperature. For gels with 20, 30, and 50 wt % SOS(3−35−3), samples were preannealed at ca. 140 °C for 1 h, and annealed for 5 min on the beamline before measurements were taken. Two-dimensional scattering patterns were recorded by a Mar-CCD area detector, and then azimuthally integrated to give one-dimensional scattering data in the form of intensity (I) versus wave vector (q). The X-ray wavelength was 0.7293 Å, and the sample-to-detector distance was 6.12 m.

RESULTS AND DISCUSSION

Gelation of SOS Triblock Copolymers in [EMI][TFSA]. The dynamic storage (G') and loss (G'') moduli for the ion gel with 10 wt % SOS(3−35−3) were measured over the temperature range from 30 to 160 °C. At each temperature, strain sweeps were conducted first to determine the linear viscoelastic regime. The loss tangent (tan δ) spectra were shifted horizontally using time−temperature superposition (tTS), and the same shift factors were applied to the dynamic moduli to obtain master curves as a function of reduced frequency, as shown in Figure 1. A liquid-like behavior is observed at temperatures above 50 °C, as evidenced by the crossover between G' and G'', and the power

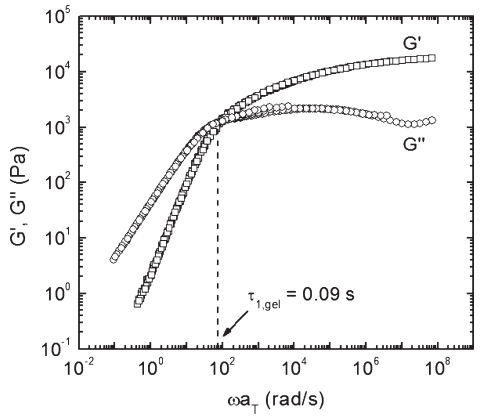

Figure 1. tTS master curves of dynamic storage and loss moduli referenced to 120 °C for the ion gel with 10 wt % SOS(3−35−3).

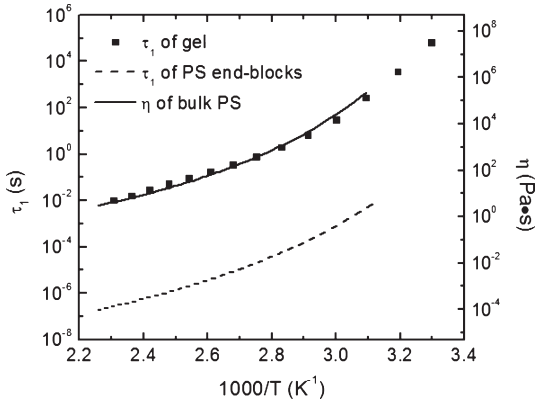

Figure 2. Temperature dependent terminal relaxation times ($\tau_{1,gel}$) of the ion gel with 10 wt % SOS(3−35−3). The viscosity data of a bulk PS sample (η) and the estimated longest relaxation time of the PS end-blocks in the SOS chains ($\tau_{1,PS}$) are presented for comparison. The bulk PS viscosity data were shifted to lower temperatures by 56 K, assuming a reduction in T_g of the micellar PS cores from bulk PS.

law exponents of two and one for G' and G'' versus ω, respectively. This result is qualitatively similar to that reported previously for a similar ion gel with 10 wt % SOS(3.3−20−3.3).[41]

The terminal flow behavior of this ion gel can be explained by transient network theory.[46] The rheological behavior of transient networks formed by swelling an ABA triblock copolymer in a B-selective solvent has been extensively studied.[47−50] Under conditions where the association strength of the A chains is weak enough to allow them to reversibly associate with and dissociate from the cross-linking points, either by thermal motion or by tension, a transient ABA network is formed. Its viscoelastic properties depend strongly on the terminal relaxation time, $\tau_{1,gel}$. With 10 wt % SOS(3−35−3), the end-blocks are short enough to enable access to the terminal flow regime of the ion gel within the experimental time scale. At the reference temperature of 120 °C, $\tau_{1,gel}$ is 0.09 s, as determined by the crossover frequency (ω_c) at which G' and G'' values are equal (Figure 1).

To further examine the exchange dynamics of the PS blocks, the values of $\tau_{1,gel}$ at various temperatures were calculated from the horizontal shift factors (a_T) used to superpose tan δ, and plotted in Figure 2 (left axis). The temperature-dependent viscosity of bulk PS(3.4) taken from ref 51 is also shown for comparison (right axis). It is evident that the temperature dependence of $\tau_{1,gel}$ closely tracks that of the bulk PS viscosity, suggesting that the terminal relaxation of the gel reflects the motion of the PS chains. Note that in Figure 2 the bulk PS(3.4) (T_g = 70 °C) viscosity data taken from ref 51 were shifted to lower temperatures by 56 K, suggesting that the T_g of the PS cores is reduced to about 14 °C. This transition was not observed in the DSC thermogram,[44] likely due to the very small amount of the cross-linking cores. However, such a reduction in T_g is not unexpected considering the nanoscopic PS domains[52] and the possible plasticizing effect of the PEO/[EMI][TFSA] matrix on the PS cores.[53,54]

The terminal relaxation of the transient gel depends both on the intrinsic mobility of PS chains and on the thermodynamic penalty of pulling the PS blocks through the PEO/[EMI][TFSA] matrix. The intrinsic mobility of the chains was determined as the terminal relaxation time of bulk PS ($\tau_{1,PS}$) with a T_g of 14 °C (equivalent to that expected of the micellar cores). $\tau_{1,PS}$ was calculated from the segmental relaxation time of bulk PS[55] (τ_{seg}) and the empirical relationship $\tau_{1,PS}/\tau_{seg} \sim N_{PS}^2$, where N_{PS} is the degree of polymerization for the PS blocks, which is 27 for the SOS in this case.[56] In Figure 2, $\tau_{1,PS}$ was plotted together with $\tau_{1,gel}$ for comparison. As expected, the temperature dependences of $\tau_{1,PS}$ and $\tau_{1,gel}$ are similar. However, $\tau_{1,gel}$ is more than 4 orders of magnitude larger than $\tau_{1,PS}$. This dynamic difference can be attributed to the energy barrier for the PS blocks to dissociate and diffuse into the PEO/[EMI][TFSA] matrix, which depends on the incompatibility χN_{PS} between PS and the matrix, where χ is the Flory−Huggins interaction parameter.[54] According to this "hindered diffusion" mechanism, the diffusion coefficient is given by[57−60]

$$D \sim D_0 \exp(-\alpha\chi N_{PS}) \quad (1)$$

where D_0 is the diffusion coefficient in the absence of any interactions and α is a constant of order unity. From eq 1, the terminal relaxation time of the gel can be expressed as

$$\tau_{1,gel} \sim \tau_{1,PS} \exp(\alpha\chi N_{PS}) \quad (2)$$

The value of $\alpha\chi$ is about 0.39, which agrees with that reported previously (0.38) for the ion gel with 10 wt % SOS(3.3−20−3.3).[41]

Rheology of SOS Gels with a Body-Centered Cubic (BCC) Structure. As the SOS content is increased to 20 wt %, terminal relaxation behavior is no longer observed. Instead, the system remains an elastic solid ($G' > G''$) over the entire measured temperature and frequency ranges, as shown by the tTS master curves in Figure 3a. Further increases in the SOS content up to 50 wt % yield similar master curves, with two plateaus evident in the storage modulus (Figure 3). The crossover frequency from one plateau to the other appears to be concentration independent, and agrees with ω_c for the gel with 10 wt % SOS(3−35−3) (corresponding to $\tau_{1,gel} \sim$ 0.09 s at 120 °C). This suggests that the rate at which PS blocks can be reversibly pulled out or inserted into the micellar cores does not vary much with polymer content over the composition range examined. These features are qualitatively similar to those observed in transient hydrogels formed by PEO based triblock copolymers.[61]

At frequencies greater than ω_c, the PS chains cannot overcome the energy barrier to diffuse into the PEO/[EMI][TFSA] matrix, and G' exhibits the rubbery plateau of the cross-linked network. Since G' in the plateau region cannot be strictly horizontal, different methods have been developed to define the plateau

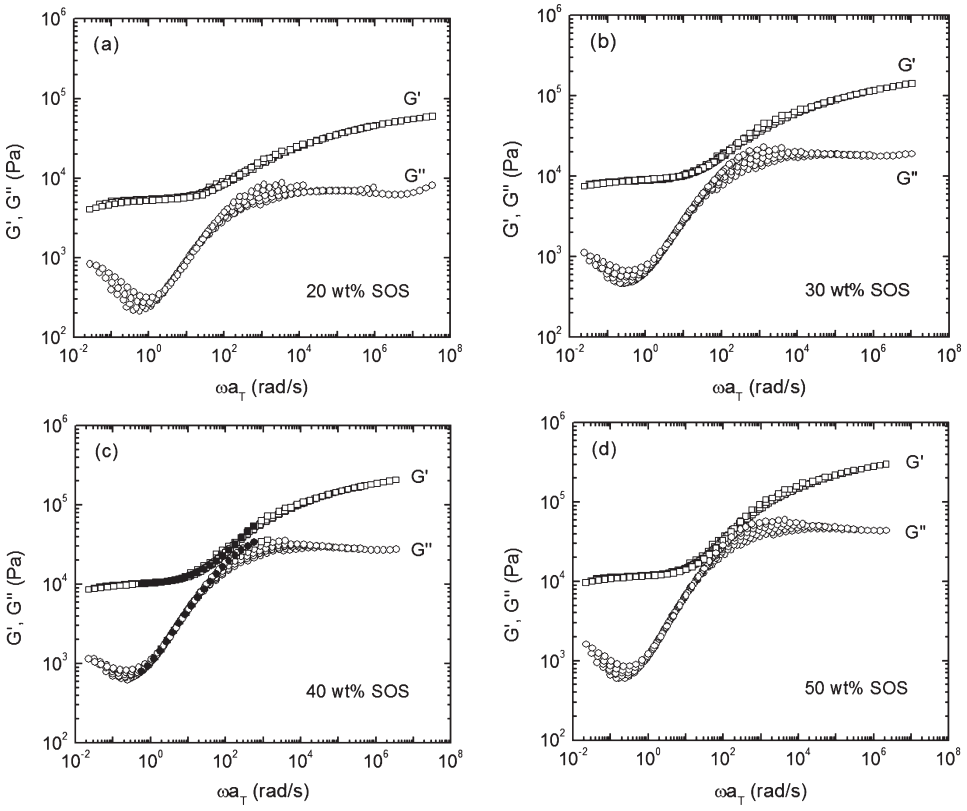

Figure 3. tTS master curves of dynamic storage and loss moduli referenced to 120 °C for ion gels with (a) 20 wt %, (b) 30 wt %, (c) 40 wt %, and (d) 50 wt % SOS(3−35−3). Filled symbols in part c denote the moduli measured at 90 °C.

modulus (G_N).[62,63] Here G_N was determined as the value of G' at the frequency where the corresponding curve of tan δ (Figure S1 in Supporting Information) has a minimum or smallest value above ω_c. The results are plotted versus SOS weight fraction on a logarithmic scale in Figure 4. A power law fit gives a slope of 2.0 ± 0.1, which agrees very well with the value of 2 reported previously for PEG-based hydrogels with polymer concentrations ≤17 wt %.[64] Experimentally determined exponents for other polymer solutions range from 2 to 2.5.[62,65] Theory anticipates a value of 2.3 for entangled solutions of neutral polymers in good solvents.[66]

According to linear viscoelastic theory, G_N can be expressed as[56]

$$G_N = \nu k_B T \tag{3}$$

where ν is the number density of network strands, k_B is the Boltzmann constant, and T is absolute temperature. For an ideal gel where every midblock is elastically effective, $\nu = cN_A/M_x$, where c is the concentration of the block copolymer in w/v, N_A is Avogadro's number, and M_x is the molecular weight between cross-links. Therefore, eq 3 can be written as

$$G_N = \frac{cfRT}{M_x} \tag{4}$$

where f is the fraction of bridging or effective midblocks inside the copolymer and R is the ideal gas constant. For the SOS gels, M_x is the molecular weight between entanglements along the PEO chains. Therefore, we estimate $M_x = M_{e,\,PEO}/w_{SOS}$, where $M_{e,\,PEO}$ is the entanglement molecular weight of melt PEO, which is 1.6 kDa at 140 °C,[67] and w_{SOS} is the weight fraction of

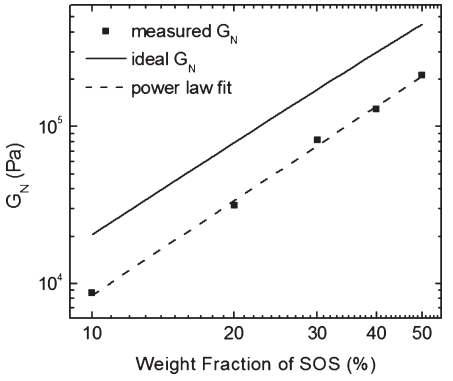

Figure 4. Concentration dependence of plateau modulus (G_N) for ion gels with 10−50 wt % SOS(3−35−3). The solid line displays the storage modulus calculated from eq 4 for ideal gels. The dashed line indicates a power law fit to the measured data.

SOS in the gel. Assuming all PEO chains bridge two cross-linking cores instead of looping back to the same one ($f = 1$), the values of G_N at 40 °C (the temperature at which the measured plateau modulus was extracted) were calculated and plotted as a solid line in Figure 4. The calculated values are about twice of the measured ones. At the low concentration end, this difference is reasonable and is comparable to previously reported transient gels.[39,44,64,68] At the high concentration end, however, this difference is perhaps more surprising: in the limit of many entanglements, e.g., ca. 11 entanglements per PEO chain with 50 wt % SOS(3−35−3), looped midblocks should contribute to the modulus almost the

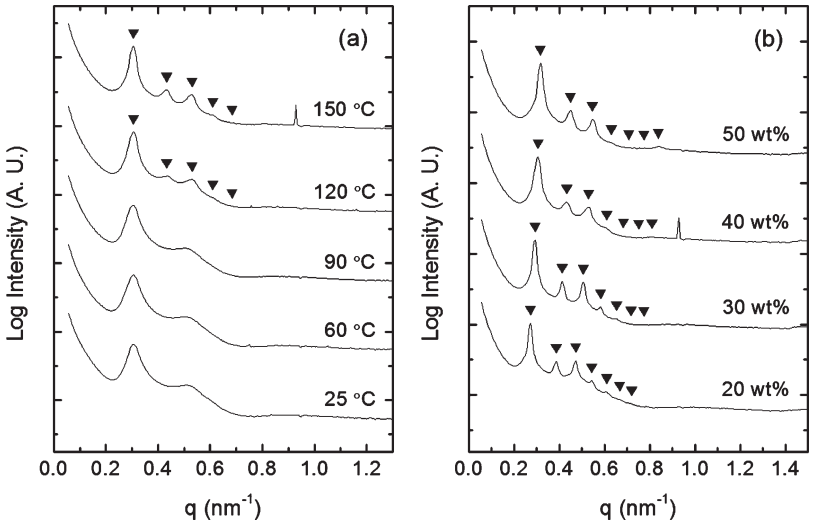

Figure 5. 1D SAXS profiles for (a) the ion gel with 40 wt % SOS(3−35−3) measured upon heating and (b) ion gels with 20, 30, and 50 wt % SOS(3−35−3) at 140 °C, and ion gel with 40 wt % SOS(3−35−3) at 150 °C. Filled triangles correspond to expected intensity maxima for BCC at q/q^* values of $1{:}\sqrt{2}{:}\sqrt{3}{:}\sqrt{4}{:}\sqrt{5}{:}\sqrt{6}{:}\sqrt{7}$.

same as bridging midblocks, and the measured modulus would be expected be closer to that of the ideal gel.

At frequencies below ω_c, the time scale is long enough (or the temperature is high enough) for the PS chains to be pulled out from the cross-links, forming a viscoelastic solution of congested micelles with PS cores and PEO coronas. This partially relaxes the stress of the system and thus brings a second, lower value modulus plateau into the measurable frequency window (Figure 3). SAXS measurements were performed to examine the morphology of the micelle solutions and solid-state gels. Figure 5a shows the SAXS profiles of the gel with 40 wt % SOS(3−35−3) upon heating. Below 90 °C, no clear ordering of the PS cores is observed. Above 90 °C, well-defined peaks appear at low q, which correspond to the Bragg reflections of a BCC structure. Once the arrangement of the micelles reaches the thermodynamically favorable state (in this case a BCC lattice) under certain conditions, such as heating, the system retains this structure after those conditions are removed (see Figure S2 in the Supporting Information for the scattering profiles of the same gel upon cooling). This suggests that kinetics is the limiting factor for the ordering of the PS micelles. The temperature above which ordering can easily occur agrees with the rheology results: at 90 °C the moduli are at the transition between the two plateaus, as shown by the filled symbols in Figure 3c.

Since the SOS(3−35−3) polymers have very long midblocks relative to the core, it is reasonable that they pack on a BCC lattice.[53,54,69] Quantities related to the length scale and structure of the gels can be extracted from the scattering profiles. The domain spacing (d_{110}) of all gels can be calculated using the profiles measured at 140 °C (Figure 5b) as $d_{110} = 2\pi/q^*$; values are listed in Table 1. This gives a lattice constant of $a = \sqrt{2}d_{110}$. The aggregation number (N_{agg}), defined here as the number of end-blocks inside a micelle, is therefore

$$N_{agg} = \nu_c a^3 = \frac{cN_A}{M_n}\left(\frac{2\sqrt{2}\pi}{q^*}\right)^3 \quad (5)$$

where ν_c is the number density of the triblock copolymer and M_n is the number-average molecular weight of the triblock, which is 40.6 kDa for the SOS polymer. Note that eq 5 assumes that all micelles pack on a BCC lattice, which is not the case as indicated by the contribution of liquid-like scattering to the peaks in the SAXS profiles. However, the average number densities of micelles in ordered versus disordered regions are expected to be similar, and thus the extracted values are still useful. It was found that d_{110} decreases with polymer concentration and N_{agg} increases, over the whole composition range studied (Table 1). This suggests that as more polymer is added, more chains aggregate in each micelle, and the number of bridging PEO strands increases, leading to a contracted BCC lattice.

The distance between the centers of two nearest PS cores, d_{nn}, can also be computed

$$d_{nn} = \frac{\sqrt{6}}{2}\frac{2\pi}{q^*} = \frac{\sqrt{3}a}{2} \quad (6)$$

which has the same concentration dependence as d_{110} (Table 1). Because core scattering is not very strong at 140 °C (Figure 5b), the core radius, R_c, was estimated from the volume of the core assuming no solvent penetration (Table 1):

$$\frac{4\pi R_c^3}{3} = \frac{2M_{n,PS}N_{agg}}{\rho_{PS}} \quad (7)$$

where $M_{n,PS}$ is the number-average molecular weight of the PS block, which is 2.8 kDa for the polymer in question, and ρ_{PS} is the density of PS, which is taken to be 1.05 g/cm^3.

The viscoelastic behavior of the congested micelles below ω_c (Figure 3) is similar to that of block copolymer/molecular solvent mixtures that adopt a cubic micellar phase, i.e., G' is essentially independent of frequency, while G'' passes through a minimum.[70] This characteristic plateau modulus associated with cubic phases (G_{cubic}) has also been suggested to be a universal feature for diblock copolymer melts.[71] Furthermore, the same report found that G_{cubic} of the melts with a BCC lattice depends on domain spacing as $G_{cubic}/RT \sim {d_{110}}^{-3.14}$. A similar correlation between G_{cubic} and d_{110} for block copolymer melts and concentrated micelle solutions has also been proposed, with each sphere per unit volume contributing $18k_BT$ to the modulus at the

Table 1. Extracted Parameters from the SAXS Profiles of the SOS Ion Gels at 140 °C

SOS content (wt %)	d_{110} (nm)	N_{agg}	d_{nn} (nm)	R_c (nm)
20	22.9 ± 0.2	143 ± 4	28.0 ± 0.2	5.3
30	21.5 ± 0.2	171 ± 4	26.3 ± 0.2	5.6
40[a]	20.5 ± 0.2	193 ± 4	25.1 ± 0.2	5.9
50	19.8 ± 0.2	209 ± 5	24.2 ± 0.2	6.0

[a] Measured at 150 °C.

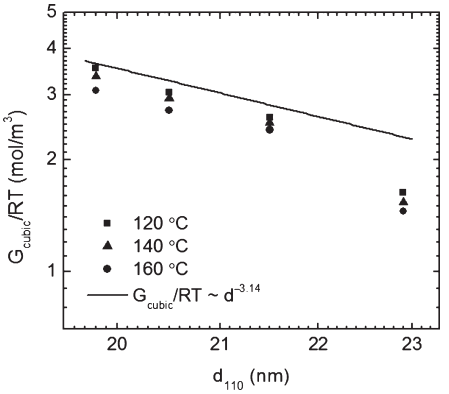

Figure 6. G_{cubic}/RT versus domain spacing (d_{110}) for ion gels with 20−50 wt % SOS(3−35−3) at selected temperatures. The solid line displays the relationship between G_{cubic}/RT and d_{110} for diblock copolymer melts with a BCC structure reproduced from ref 71.

order−disorder transition temperature (T_{ODT}).[72] The power law relation in ref 71 is plotted in Figure 6, along with the experimentally measured values for the SOS gels at three temperatures at which the system can be considered a micellar solution. By analogy to G_N, the measured G_{cubic} was determined as the value of G' at the frequency where the corresponding curve of tan δ has a minimum at the indicated temperatures (Figure S1 in the Supporting Information). For a particular concentration, the value of G_{cubic}/RT only decreases slightly with increasing temperature (<15% over 40 °C). Even though the measured range of d_{110} is too small to compare the power law dependence, the corresponding G_{cubic}/RT values of the SOS system agree very well with those of the diblock copolymer melts with the same d_{110}. This indicates that the incorporation of [EMI][TFSA] into the PEO domain can be qualitatively regarded as increasing the volume fraction of the PEO chains, which makes the micellar solution similar to a hypothetical SO diblock melt having the measured domain spacing values.

Comparison of SOS and SMS Gels. Figure 7 displays the modulus master curves of the SMS and SOS gels with 40 wt % polymer referenced to 120 °C. Qualitatively, both gels exhibit two "plateau" regions: one with larger modulus at high frequencies (low temperatures) and the other with smaller modulus at low frequencies (high temperatures). This feature is universal for gels with polymer concentrations of 20−50 wt %. Although G' of both the SMS and SOS gel decreases by approximately equal amounts (more than an order of magnitude) over the frequency range shown, the relaxations that account for this drop are fundamentally different for the SMS and SOS gels. For the SMS gel, the drop in G' is gradual and occurs over the entire frequency range. Comparison of this gel with a PMMA

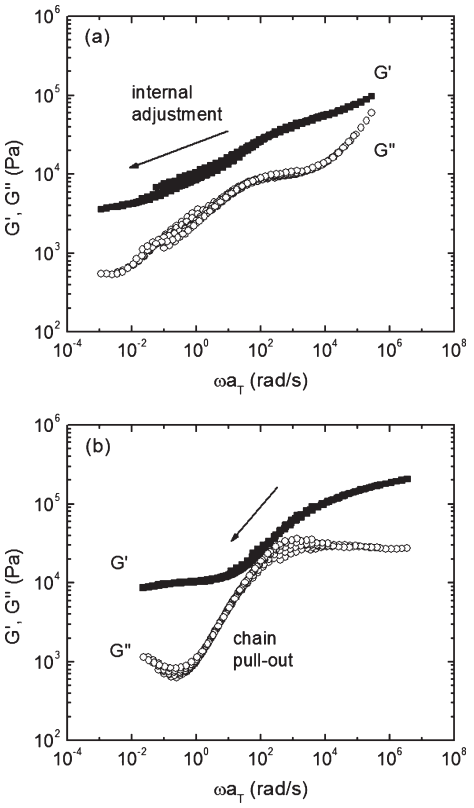

Figure 7. Master curves of storage and loss moduli referenced to 120 °C for ion gels with (a) 40 wt % SMS(18−86−18) and (b) 40 wt % SOS(3−35−3).

homopolymer solution showed that the decrease in G' from ca. 10^5 to 3×10^4 Pa (corresponding to a frequency range of ca. 3×10^5 to 100 rad/s in Figure 7a) is mainly due to the relaxation of PMMA strands within the ionic liquid, and further decrease in G' can be attributed to the relaxation of the PS chains.[44] On the other hand, the drop in G' for the SOS gel is much sharper, and occurs mostly within 2 orders of magnitude in reduced frequency. This can be ascribed to the pull out of the PS chains. The difference in the behavior of the PS end-blocks for the SMS and SOS gels are due to the different lengths of the PS end-blocks. For the SMS gel, the end-blocks are long, resulting in a large χN_{PS}. This large thermodynamic barrier makes it unlikely for the PS blocks to be pulled out from the cross-linking cores. Therefore, the system maintains its network structure at elevated temperatures (corresponding to frequencies below 100 rad/s in Figure 7a), and the gradual decrease in modulus is due primarily to the motions of PS chains within the cores, and that of the cores within a disordered medium. Thus, G' is greater than G'' throughout the frequency range. On the other hand, since the PS blocks of the SOS are short (small χN_{PS}), the PS chains can dissociate from the cores and diffuse into the PEO/[EMI][TFSA] matrix at high temperatures, resulting in a viscoelastic micelle solution without a persistent network structure. The chain pull-out is evidenced by the terminal behavior for G' and G'' in the 10% solution (Figure 1) (which corresponds well to the frequency range of the drop in G' at higher concentrations), and the fact that upon annealing the system can reach the thermodynamically favorable BCC packing.

Ionic Conductivity. Since the PS blocks are introduced mainly to provide mechanical support to the ion gels, it is important to

understand the effect they exert on ionic conduction. Figure 8 displays the ionic conductivity ratio ($\sigma_{gel}/\sigma_{solution}$) of both the SOS and the previously reported SMS gels to homopolymer solutions having similar PEO or PMMA content, versus the volume fraction of the PS micelles. The total polymer concentrations range from 5−50 wt %, and the selected temperatures vary from 25 to 200 °C. Consequently, the actual conductivities vary by over a factor of 400 (Table S1 in Supporting Information). However, the reduction of σ for the gels with respect to the equivalent solutions is within a factor of 2.1 for both triblocks over the entire composition and temperature ranges investigated, and $\sigma_{gel}/\sigma_{solution}$ decreases with increasing volume fraction of PS micelles. This important result highlights the fact that the act of introducing the micellar cross-links has a negligible effect on conductivity, while the effect on the low frequency modulus is dramatic.

The dependence of $\sigma_{gel}/\sigma_{solution}$ on the volume fraction of PS agrees well with the prediction based on an obstruction model developed by Mackie and Meares (solid line in Figure 8).[73] In a hypothetical lattice randomly occupied by equally sized polymer chain segments and solvent molecules, assuming that solvent diffusion occurs through lattice sites unoccupied by the polymer, the ratio of diffusion coefficient in the gel (D_g) to that of the neat solvent (D_0) can be written as[74]

$$\frac{D_g}{D_0} = \left(\frac{1-\phi}{1+\phi}\right)^2 \quad (8)$$

where ϕ is the polymer volume fraction. For the ion gels, the conducting domain consists of both the midblocks and the ionic liquid, and the insulating PS cores obstruct the ion pathways. Therefore, the conducting phase is taken to be the "solvent". Assuming the number density of conducting ions is the same for the gel and the homopolymer solution, the conductivity ratio of the two can be expressed in the same way as the diffusion coefficient:

$$\frac{\sigma_{gel}}{\sigma_{solution}} = \left(\frac{1-\phi}{1+\phi}\right)^2 \quad (9)$$

The agreement between theory and experiment is quite remarkable considering the simple assumptions of the Mackie−Meares model, combined with the wide temperature and concentration ranges measured.

Materials Design Considerations. Combining the results here and those reported previously on the ion gels,[41,44] the concentration and molecular weight of the triblock can be tuned to meet specific property needs. As far as gel modulus is concerned, a higher modulus can be obtained with the addition of more polymer or using a midblock with a smaller entanglement molecular weight. Nevertheless, as the addition of polymer lowers the ionic conductivity, there is a trade-off that should be balanced. If for the sake of high modulus 20 wt % or more polymer is needed, it is better to use a flexible midblock since in this concentration range conductivity is higher for gels with a lower T_g midblock. Once the midblock is chosen, the reduction of conductivity for the gels with respect to homopolymer solutions can be minimized by making the PS end-blocks relatively short. However, in order to maintain mechanical integrity at a certain triblock concentration, the end-blocks need to be long enough to obtain a persistent gel at the desired temperature. For the SOS gels, we have reported that the molecular weight of the end-blocks needs to be at least 3.8 kDa to achieve a melting temperature above 100 °C with 10 wt % SOS.[41] On the other hand, thermoreversible gels can easily be obtained with fine-tuned gelation temperature by varying the molecular weight of the PS block.

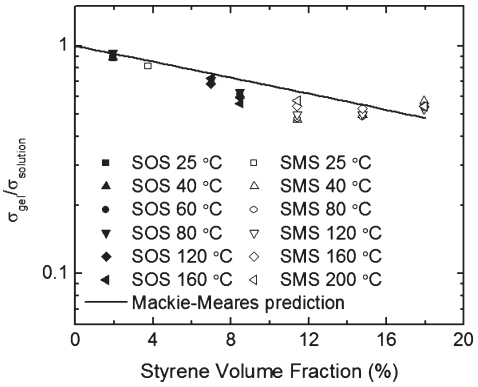

Figure 8. Ionic conductivity ratio of the ion gels to the homopolymer solutions versus the volume fraction of styrene in the gels at selected temperatures. The polymer concentrations in the gels and solutions corresponding to the styrene volume fractions from low to high are: 10 wt % SOS(3−35−3) versus 8 wt % PEO(35), 10 wt % SMS(18−86−18) versus 5 wt % PMMA(126), 40 wt % SOS(3−35−3) versus 34 wt % PEO(35), 50 wt % SOS(3−35−3) versus 43 wt % PEO(35), 30 wt % SMS(18−86−18) versus 20 wt % PMMA(126), 40 wt % SMS(18−86−18) versus 30 wt % PMMA(126), and 50 wt % SMS(18−86−18) versus 40 wt % PMMA(126).

CONCLUSIONS

We have investigated the viscoelastic properties and ionic conductivity of ion gels based on an SOS(3−35−3) triblock copolymer and the ionic liquid [EMI][TFSA] over wide ranges of temperature and composition. The ion gel with 10 wt % SOS(3−35−3) "melts" at high temperatures; its longest relaxation time tracks the temperature dependence of bulk PS viscosity, while the actual relaxation values are more than 4 orders of magnitude higher than those for bulk PS due to the energy barrier of pulling the PS end-blocks through the PEO/[EMI][TFSA] matrix. Gels with 20−50 wt % SOS(3−35−3) do not melt and show two plateaus in G'. The one above ω_c is that of the entangled network with PEO strands and PS cross-links; its value depends quadratically on polymer weight fraction and is about half of that predicted from linear viscoelastic theory due to looping. The other plateau below ω_c is that of the congested micelle solution with PS cores and PEO coronas, the value of which depends on domain spacing in a similar way as diblock melts. ω_c characterizes the time scale at which PS end-block pull-out occurs. The ionic conductivity ratio of both SOS- and SMS-based ion gels to homopolymer solutions with the same midblock content is above 0.5, and it depends on PS volume fraction following the Mackie−Meares model. Combining the considerations on modulus, ionic conductivity, and thermal stability allows rational designs of the triblock in ion gels to meet specific property requirements.

ASSOCIATED CONTENT

Supporting Information. Master curves of tan δ for the SOS ion gels, 1D SAXS profiles of the ion gel with 40 wt %

SOS(3−35−3) upon cooling, and ionic conductivity data for all the ion gels and homopolymer solutions. This material is available free of charge via the Internet at http://pubs.acs.org.

AUTHOR INFORMATION

Corresponding Author
*E-mail: (C.D.F.) frisbie@umn.edu; (T.P.L.) lodge@umn.edu.

ACKNOWLEDGMENT

This work was supported by the National Science Foundation through the MRSEC program at the University of Minnesota, Award DMR-0819885. Use of the Advanced Photon Source was supported by the U.S. Department of Energy, Office of Science, Basic Energy Sciences, under Contract DE-AC02-06CH11357. We thank Professor Philippe Buhlmann for access to his impedance spectroscopy equipment, and Brad Jones and Lucas McIntosh for their assistance with SAXS experiments.

REFERENCES

(1) Welton, T. *Chem. Rev.* **1999**, *99*, 2071–2083.
(2) Galinski, M.; Lewandowski, A.; Stepniak, I. *Electrochim. Acta* **2006**, *51*, 5567–5580.
(3) MacFarlane, D. R.; Forsyth, M.; Howlett, P. C.; Pringle, J. M.; Sun, J.; Annat, G.; Neil, W.; Izgorodina, E. I. *Acc. Chem. Res.* **2007**, *40*, 1165–1173.
(4) Wasserscheid, P.; Welton, T. *Ionic Liquids in Synthesis*, 2nd ed.; Wiley-VCH: Weinheim, Germany, 2008.
(5) Gorlov, M.; Kloo, L. *Dalton Trans.* **2008**, 2655–2666.
(6) Zakeeruddin, S. M.; Graetzel, M. *Adv. Funct. Mater.* **2009**, *19*, 2187–2202.
(7) Papageorgiou, N.; Athanassov, Y.; Armand, M.; Bonhote, P.; Pettersson, H.; Azam, A.; Grätzel, M. *J. Electrochem. Soc.* **1996**, *143*, 3099–3108.
(8) Lu, W.; Fadeev, A. G.; Qi, B.; Smela, E.; Mattes, B. R.; Ding, J.; Spinks, G. M.; Mazurkiewicz, J.; Zhou, D.; Wallace, G. G.; MacFarlane, D. R.; Forsyth, S. A.; Forsyth, M. *Science* **2002**, *297*, 983–987.
(9) Ding, J.; Zhou, D.; Spinks, G.; Wallace, G.; Forsyth, S.; Forsyth, M.; MacFarlane, D. *Chem. Mater.* **2003**, *15*, 2392–2398.
(10) Zhou, D.; Spinks, G. M.; Wallace, G. G.; Tiyapiboonchaiya, C.; MacFarlane, D. R.; Forsyth, M.; Sun, J. *Electrochim. Acta* **2003**, *48*, 2355–2359.
(11) McEwen, A. B.; Ngo, E. L.; LeCompte, K.; Goldman, J. L. *J. Electrochem. Soc.* **1999**, *146*, 1687–1695.
(12) Sato, T.; Masuda, G.; Takagi, K. *Electrochim. Acta* **2004**, *49*, 3603–3611.
(13) Ue, M.; Takeda, M.; Toriumi, A.; Kominato, A.; Hagiwara, R.; Ito, Y. *J. Electrochem. Soc.* **2003**, *150*, A499–A502.
(14) Katakabe, T.; Kaneko, T.; Watanabe, M.; Fukushima, T.; Aida, T. *J. Electrochem. Soc.* **2005**, *152*, A1913–A1916.
(15) Balducci, A.; Henderson, W. A.; Mastragostino, M.; Passerini, S.; Simon, P.; Soavi, F. *Electrochim. Acta* **2005**, *50*, 2233–2237.
(16) Lewandowski, A.; Swiderska-Mocek, A. *J. Power Sources* **2009**, *194*, 601–609.
(17) Ishikawa, M.; Sugimoto, T.; Kikuta, M.; Ishiko, E.; Kono, M. *J. Power Sources* **2006**, *162*, 658–662.
(18) Kim, G. T.; Jeong, S. S.; Joost, M.; Rocca, E.; Winter, M.; Passerini, S.; Balducci, A. *J. Power Sources* **2011**, *196*, 2187–2194.
(19) Ono, S.; Seki, S.; Hirahara, R.; Tominari, Y.; Takeya, J. *Appl. Phys. Lett.* **2008**, *92*, 103313/1–103313/3.
(20) Yuan, H.; Shimotani, H.; Tsukazaki, A.; Ohtomo, A.; Kawasaki, M.; Iwasa, Y. *Adv. Funct. Mater.* **2009**, *19*, 1046–1053.
(21) Lee, J.; Panzer, M. J.; He, Y.; Lodge, T. P.; Frisbie, C. D. *J. Am. Chem. Soc.* **2007**, *129*, 4532–4533.
(22) Cho, J. H.; Lee, J.; He, Y.; Kim, B. S.; Lodge, T. P.; Frisbie, C. D. *Adv. Mater.* **2008**, *20*, 686–690.
(23) Cho, J. H.; Lee, J.; Xia, Y.; Kim, B.; He, Y.; Renn, M. J.; Lodge, T. P.; Frisbie, C. D. *Nat. Mater.* **2008**, *7*, 900–906.
(24) Lee, S. W.; Lee, H. J.; Choi, J. H.; Koh, W. G.; Myoung, J. M.; Hur, J. H.; Park, J. J.; Cho, J. H.; Jeong, U. *Nano Lett.* **2010**, *10*, 347–351.
(25) Hanabusa, K.; Fukui, H.; Suzuki, M.; Shirai, H. *Langmuir* **2005**, *21*, 10383–10390.
(26) Mohmeyer, N.; Kuang, D.; Wang, P.; Schmidt, H. W.; Zakeeruddin, S. M.; Gratzel, M. *J. Mater. Chem.* **2006**, *16*, 2978–2983.
(27) Ueki, T.; Watanabe, M. *Macromolecules* **2008**, *41*, 3739–3749.
(28) Lodge, T. P. *Science* **2008**, *321*, 50–51.
(29) The term solid polymer electrolyte (SPE) is often used in the literature to describe viscoelastic, solvent-free polymer electrolyte systems. Here SPE only refers to systems with persistent solid structures.
(30) Lee, K. H.; Zhang, S.; Lodge, T. P.; Frisbie, C. D. *J. Phys. Chem. B* **2011**, *115*, 3315–3321.
(31) Fullerton-Shirey, S. K.; Maranas, J. K. *Macromolecules* **2009**, *42*, 2142–2156.
(32) Susan, M. A. B. H.; Kaneko, T.; Noda, A.; Watanabe, M. *J. Am. Chem. Soc.* **2005**, *127*, 4976–4983.
(33) Seki, S.; Susan, M. A. B. H.; Kaneko, T.; Tokuda, H.; Noda, A.; Watanabe, M. *J. Phys. Chem. B* **2005**, *109*, 3886–3892.
(34) Klingshirn, M. A.; Spear, S. K.; Subramanian, R.; Holbrey, J. D.; Huddleston, J. G.; Rogers, R. D. *Chem. Mater.* **2004**, *16*, 3091–3097.
(35) Neouze, M.-A.; Le Bideau, J.; Gaveau, P.; Bellayer, S.; Vioux, A. *Chem. Mater.* **2006**, *18*, 3931–3936.
(36) Matsumoto, K.; Endo, T. *Macromolecules* **2008**, *41*, 6981–6986.
(37) Matsumoto, K.; Endo, T. *Macromolecules* **2009**, *42*, 4580–4584.
(38) Jana, S.; Parthiban, A.; Chai, C. L. L. *Chem. Commun.* **2010**, *46*, 1488–1490.
(39) He, Y.; Boswell, P. G.; Buehlmann, P.; Lodge, T. P. *J. Phys. Chem. B* **2007**, *111*, 4645–4652.
(40) He, Y.; Lodge, T. P. *Chem. Commun.* **2007**, 2732–2734.
(41) He, Y.; Lodge, T. P. *Macromolecules* **2008**, *41*, 167–174.
(42) Noro, A.; Matsushita, Y.; Lodge, T. P. *Macromolecules* **2008**, *41*, 5839–5844.
(43) Noro, A.; Matsushita, Y.; Lodge, T. P. *Macromolecules* **2009**, *42*, 5802–5810.
(44) Zhang, S.; Lee, K. H.; Frisbie, C. D.; Lodge, T. P. *Macromolecules* **2011**, *44*, 940–949.
(45) Zeroni, I.; Ozair, S.; Lodge, T. P. *Macromolecules* **2008**, *41*, 5033–5041.
(46) Tanaka, F.; Edwards, S. F. *Macromolecules* **1992**, *25*, 1516–1523.
(47) Sato, T.; Watanabe, H.; Osaki, K. *Macromolecules* **2000**, *33*, 1686–1691.
(48) Vega, D. A.; Sebastian, J. M.; Loo, Y.-L.; Register, R. A. *J. Polym. Sci., Part B: Polym. Phys.* **2001**, *39*, 2183–2197.
(49) Inomata, K.; Nakanishi, D.; Banno, A.; Nakanishi, E.; Abe, Y.; Kurihara, R.; Fujimoto, K.; Nose, T. *Polymer* **2003**, *44*, 5303–5310.
(50) Seitz, M. E.; Burghardt, W. R.; Faber, K. T.; Shull, K. R. *Macromolecules* **2007**, *40*, 1218–1226.
(51) Plazek, D. J.; O'Rourke, V. M. *J. Polym. Sci., Polym. Phys. Ed.* **1971**, *9*, 209–143.
(52) Roth, C. B.; Dutcher, J. R. *J. Electroanal. Chem.* **2005**, *584*, 13–22.
(53) Lai, C.; Russel, W. B.; Register, R. A. *Macromolecules* **2002**, *35*, 841–849.
(54) Choi, S.-H.; Bates, F. S.; Lodge, T. P. *J. Phys. Chem. B* **2009**, *113*, 13840–13848.
(55) He, Y.; Lutz, T. R.; Ediger, M. D.; Ayyagari, C.; Bedrov, D.; Smith, G. D. *Macromolecules* **2004**, *37*, 5032–5039.
(56) Hiemenz, P. C.; Lodge, T. P. *Polymer Chemistry*, 2nd ed.; CRC Press: New York, 2007.
(57) Yokoyama, H.; Kramer, E. J. *Macromolecules* **1998**, *31*, 7871–7876.
(58) Cavicchi, K. A.; Lodge, T. P. *Macromolecules* **2003**, *36*, 7158–7164.

(59) Choi, S.-H.; Lodge, T. P.; Bates, F. S. *Phys. Rev. Lett.* **2010**, *104*, 047802/1–047802/4.
(60) Choi, S.-H.; Bates, F. S.; Lodge, T. P. *Macromolecules* **2011**, *44*, 3594–3604.
(61) Renou, F.; Nicolai, T.; Benyahia, L.; Nicol, E. *J. Phys. Chem. B* **2009**, *113*, 3000–3007.
(62) Tao, H.; Huang, C.; Lodge, T. P. *Macromolecules* **1999**, *32*, 1212–1217.
(63) Graessley, W. W. *Adv. Polym. Sci.* **1974**, *16*, 1–179.
(64) Tae, G.; Kornfield, J. A.; Hubbell, J. A.; Lal, J. *Macromolecules* **2002**, *35*, 4448–4457.
(65) Mok, M.; Liu, X.; Bai, Z.; Lei, Y.; Lodge, T. P. *Macromolecules* **2011**, *44*, 1016–1025.
(66) Colby, R. H. *Rheol. Acta* **2010**, *49*, 425–442.
(67) Fetters, L. J.; Lohse, D. J.; Richter, D.; Witten, T. A.; Zirkel, A. *Macromolecules* **1994**, *27*, 4639–4647.
(68) Annable, T.; Buscall, R.; Ettelaie, R.; Whittlestone, D. *J. Rheol.* **1993**, *37*, 695–726.
(69) McConnell, G. A.; Gast, A. P.; Huang, J. S.; Smith, S. D. *Phys. Rev. Lett.* **1993**, *71*, 2102–2105.
(70) Hamley, I. W. *Philos. Trans. R. Soc. A* **2001**, *359*, 1017–1044.
(71) Kossuth, M. B.; Morse, D. C.; Bates, F. S. *J. Rheol.* **1999**, *43*, 167–196.
(72) Sebastian, J. M.; Lai, C.; Graessley, W. W.; Register, R. A. *Macromolecules* **2002**, *35*, 2707–2713.
(73) Mackie, J. S.; Meares, P. *Proc. R. Soc. London* **1955**, *A232*, 498–509.
(74) Amsden, B. *Macromolecules* **1998**, *31*, 8382–8395.